Research Square

Preprints are preliminary reports that have not undergone peer review.
They should not be considered conclusive, used to inform clinical practice,
or referenced by the media as validated information.

Visual-Navigation-Aware Multi-UAV Waypoint Assignment for Border Surveillance in GNSS-Denied Environments

Jean Marie Vianney ISHIMWE

jmvishimwefils@gmail.com

Cranfield University

Sabyasachi Mondal

Cranfield University

Antonios Tsourdos

Cranfield University

Research Article

Keywords:

Posted Date: November 11th, 2026

DOI: https://doi.org/10.21203/rs.3.rs-11472879/v1

License: This work is licensed under a Creative Commons Attribution 4.0 International License.
Read Full License

Additional Declarations: No competing interests reported.

Visual-Navigation-Aware Multi-UAV Waypoint Assignment for Border Surveillance in GNSS-Denied Environments

Jean Marie Vianney ISHIMWE[1*], Sabyasachi Mondal[1] and Antonios Tsourdos[1]

[1*] Faculty of Engineering and Applied Sciences, Cranfield University, Cranfield, United Kingdom .

*Corresponding author(s). E-mail(s): jmvishimwefils@gmail.com;

Abstract

Uncrewed Aerial Vehicle (UAV) swarms using visual navigation methods for border surveillance in Global Navigation Satellite System (GNSS)-denied environments have to maintain positional accuracy with recognisable visual features to reduce the risk of being lost en route. A scarcity of visually rich textures is more likely in rural border environments which makes judicious route planning important for successful visual navigation. Existing multi-UAV routing formulations mainly optimise distance, time, or coverage without deeply considering limited key features terrain for visual navigation. This work formulates a waypoint-assignment problem in which terrain navigability and border surveillance coverage are jointly considered. A terrain navigability framework is constructed from operational orthomosaic imagery using Scale-Invariant Feature Transform (SIFT) feature density and response quality. Candidate observation positions are extracted from the constructed navigability map and routes are evaluated using an A^* planner. The assignment problem is formulated as a single-depot open min–max multiple Travelling Salesman Problem (mTSP) with two objectives: weakest-link route reliability and swarm union border coverage. Two independent solvers, Non-dominated Sorting Genetic Algorithm II with A-Star Search Algorithm (NSGA-II + A^*) and Genetic Algorithm for the Multiple Traveling Salesperson Problem with A-Star Search Algorithm (GA-mTSP + A^*), are evaluated with the same routing mechanism. Under the baseline configuration, both approaches achieve approximately **91.0%** border coverage, with route-reliability scores of 0.3770 and 0.3707, respectively. Both identify five UAVs as the optimal swarm size under the baseline configuration and NSGA-II requires less computation time.

Keywords: UAV swarm, visual navigation, GNSS-denied navigation, waypoint assignment, path planning, multi-objective optimisation

1 Introduction

Border surveillance remains a challenge for national security agencies. Traditional methods like fixed infrastructure towers for human observation or patrols are costly and risky to human life and may leave gaps in coverage [1]. UAV swarms provide an alternative solution; several aircraft can be deployed to conduct surveillance widely over remote and difficult terrain. However, uncrewed systems that rely only on Global Navigation Satellite Systems (GNSS) for navigation are vulnerable in contested environments. GNSS signal jamming equipment is becoming easily accessible at low cost [2, 3], when GNSS signals are unavailable or degraded, conventional navigation may become unreliable. Visual navigation provides an alternative to conventional navigation by estimating vehicle position and motion from visual information available in the environment. There are different visual navigation techniques: feature-based localisation, visual odometry, simultaneous localisation and mapping (SLAM), and visual-inertial odometry and all depend on the availability of recognisable visual content for confident navigation.

Vision-based navigation has been widely investigated as an alternative to GNSS-dependent navigation. Existing approaches include feature-based localisation, visual odometry, SLAM, and visual inertial odometry [4–7]. ORB-SLAM2 uses ORB features for tracking, mapping, and loop closure [8], while VINS-Mono combines monocular imagery and inertial measurements for visual inertial state estimation [9]. These methods also depend on sufficient visual information available in the surrounding environment [10]. Feature scarcity can degrade tracking and localisation, while perceptual aliasing can cause different physical locations to produce similar observations looking [11]. Position errors can also be accumulated over long flight paths under outdoor conditions [12], which proves that terrain visual richness is directly related to the reliability of visual navigation. Poor visual environments such as open agricultural fields contain fewer features which are unreliable for feature matching and localisation correction. Visual navigation remains limited to feature scarcity, perceptual aliasing, and accumulated drift [5, 11, 12].

For a UAV swarm conducting surveillance over rural border terrain, these limitations have a direct consequence on this mission: a judicious planning for the route that remains close to visually rich permanent features such as roads, woodland boundaries, rivers, and field margins could improve the reliability of visual localisation compared to a route through homogeneous terrain. Therefore, the problem is not only how to improve the onboard navigation algorithm but also how to plan the route that keeps the robots through recognisable key features and the selection of terminal observation points that support reliable visual navigation. Traditional path planners such as A^* minimise the distance of the flight or path costs [13]. This cost representation can be modified in favour of navigation through regions that provide better localisation opportunities. Landmark-aware and perception-aware planning has demonstrated

that routes to the same destination can provide different localisation quality [14, 15]. However, several existing approaches rely on artificial installed landmarks or consider perception during trajectory generation rather than pre-mission waypoint assignment with orthometric imagery.

Existing multi-UAV routing and surveillance methods mainly have considered different approaches such as route length, workload distribution, coverage, and landmark-assisted navigation [14, 16–18]. These methods generally assume that destinations are predefined, all nodes are to be visited, or candidate locations are equally navigable. The problem considered within this work is different: only K observation positions must be selected from N candidates, and the routes to those positions must simultaneously support visual navigation and surveillance coverage. Multi-objective optimisation-based frameworks such as the mTSP [19, 20] and NSGA-II have been used for assigning routes to multiple agents [21]. Especially, NSGA-II performs multi-objective optimisation using non-dominated sorting and crowding distance and it has been widely used in UAV path planning and swarm task allocation [22, 23]. To the authors' knowledge, existing multi-UAV waypoint-assignment approaches have not jointly considered terrain visual navigability, selective observation-point assignment, calibration point spacing, and collective surveillance coverage within a single pre-mission planning framework.

2 Research Contributions

This research addresses the identified gap through a pre-mission planning framework that uses orthometric imagery and pre-extracted SIFT keypoint data to score terrain visual quality, plan routes that pass through visually recognisable terrain, and assign observation waypoints that collectively maximise border surveillance coverage. The main contributions are:

1. A terrain visual-navigability scoring formulation that combines SIFT feature quantity and response quality:

$$\mathrm{ScoreGrid}(c) = \mathrm{COUNT}(c)\left[1 + \overline{\mathrm{ResponseNorm}}(c)\right]. \tag{1}$$

   The contribution is not the use of SIFT itself but the use of pre-extracted SIFT keypoints to construct a terrain visual-navigability representation for pre-mission UAV route planning. The formulation combines both feature density and response quality within each terrain cell, allowing visually rich and visually poor regions to be distinguished before flight. In this context, visual information from the orthometric imagery becomes an input to the route planning process rather than being considered only during onboard visual navigation.
2. A selective K size from N waypoint-assignment formulation so that terrain visual navigability and border surveillance coverage are both considered. Unlike conventional multi-UAV routing problems in which destinations are predefined or all candidate nodes are required to be visited, this formulation selects only K size as observation positions from N available candidates and assigns them to the UAV

swarm. The contribution in this context is the joint consideration of the visual navigability of the routes leading to the selected observation positions and the collective border surveillance coverage provided by those positions. Therefore, waypoint selection, route planning, and surveillance coverage are considered together rather than as independent planning problems.

3. A route-reliability objective that penalises large spacing between recognisable calibration points to avoid large drifting. The contribution extends terrain visual navigability by considering not only the visual quality of the terrain along a route but also the spacing between recognisable calibration points. A route may contain visually rich regions while still including long sections with limited opportunities for visual localisation correction. The proposed spacing penalty therefore reduces the reliability score of routes containing large gaps between recognisable calibration points. The weakest route among the UAVs is then considered in the optimisation so that high overall surveillance coverage is not achieved at the expense of assigning one UAV a visually unreliable route.

3 Problem Formulation

Given a UAV swarm of size (K) departs from a common secure base and has to reach the static observation positions along a border for surveillance. Each UAV relies on visual navigation, which works by tracking and matching visually recognisable permanent terrain features. Let us consider

$$V = \{v_1, \ldots, v_N\} \tag{2}$$

representing the candidate waypoints set and

$$V_{\text{border}} \subseteq V \tag{3}$$

represent the candidates capable of being observation points along the border. The binary assignment variable is

$$z_{ik} = \begin{cases} 1, & \text{if node } v_i \text{ is assigned to UAV } k, \\ 0, & \text{otherwise.} \end{cases} \tag{4}$$

Each UAV receives one terminal:

$$\sum_{i \in V} z_{ik} = 1, \qquad k = 1, \ldots, K, \tag{5}$$

and no observation point can be shared:

$$\sum_{k=1}^{K} z_{ik} \leq 1. \tag{6}$$

The assigned terminal points must belong to: V_{border}.

3.1 Route Reliability

For UAV size k, the route from the base b to the terminal w_k is

$$R_k = A^*(b, w_k). \tag{7}$$

navigable, and route navigability is defined such that it combines intermediate waypoints' distinctiveness and terrain quality such that:

$$\text{nav}(R_k) = \alpha Q_{\text{nodes}}(R_k) + (1-\alpha) Q_{\text{terrain}}(R_k). \tag{8}$$

The mean distance between recognisable calibration opportunities is:

$$\delta_k = \frac{d(R_k)}{m(R_k)+1}, \tag{9}$$

where $d(R_k)$ is the route distance and $m(R_k)$ the number of intermediate recognised nodes. The route is penalised when δ_k exceeds the desired calibration distance Δ^* such that:

$$\lambda_k = \begin{cases} 1, & \delta_k \leq \Delta^*, \\ \exp[-\gamma(\delta_k - \Delta^*)], & \delta_k > \Delta^*. \end{cases} \tag{10}$$

The final route reliability is then defined as:

$$S_k = \text{nav}(R_k)\lambda_k. \tag{11}$$

The first objective is the weakest UAV route:

$$f_1 = \min_{k=1,\ldots,K} S_k. \tag{12}$$

3.2 Border Coverage

Each UAV at its assigned observation position covers an interval, I_k and the collective coverage objective is:

$$f_2 = \frac{\left|\bigcup_{k=1}^{K} I_k\right|}{L}, \tag{13}$$

where L is the total length of the border. Therefore the optimisation aims for:

$$\max(f_1, f_2). \tag{14}$$

4 Methodology

4.1 Dataset and Feature Registration

The operational orthomosaic image consisted of 361 image tiles arranged in a 19×19 grid. Each greyscale image has 1750×1750 pixels which make a complete operational

image of 33250×33250 pixels. Each tile contained 10,000 pre-extracted SIFT keypoints, giving approximately 3.61 million features, and all were registered with their coordinate system according to the corresponding tile location in pixels.

4.2 Terrain Navigability Map

SIFT response values were normalised per tile such that:

$$R_i^{\text{norm}} = \frac{R_i - R_{t,\min}}{R_{t,\max} - R_{t,\min}}. \tag{15}$$

The complete operational map was then divided into cells of 175×175 pixels, resulting in 190×190 grid. The navigability score in Eq. (1) was normalised to the range $[0, 1]$ such that the cell with the strongest visual response was assigned a navigability score of 1:

$$\text{NavGrid}(c) = \frac{\text{ScoreGrid}(c)}{\max_c \text{ScoreGrid}(c)}. \tag{16}$$

Hence,

$$0 \leq \text{NavGrid}(c) \leq 1,$$

where a value close to 1 represents highly recognisable feature terrain, while a value close to 0 represents terrain with weak visual distinctiveness. The traversal cost was then defined as:

$$\text{CostGrid}(c) = 1 - \text{NavGrid}(c), \tag{17}$$

such that the highly visual navigable terrain produces a low traversal cost and poorly recognisable terrain produces a high traversal cost. Only 318 of the 36,100 terrain cells had

$$\text{NavGrid} \geq 0.5,$$

indicating that highly recognisable terrain was sparsely distributed and scarce.

4.3 Candidate Waypoint Extraction and Routing

Candidate observation point nodes are extracted from the constructed NavGrid with the characteristic of being locally distinctive within their terrain cell. The extraction procedure consists of three steps: local maxima detection, score thresholding, and non-maximum suppression.

4.3.1 Local Maxima Detection

Candidate nodes have been selected as the cell whose NavGrid score exceeds their neighbours in the 190×190 grid. This was implemented using `imregionalmax(NavGrid)` in MATLAB, which returns a binary mask and marks every regional cell that are higher than all other connected neighbours in eight direction neighbourhood. This regional maxima represent the terrain patches that are more visually distinctive than their immediate surroundings.

4.3.2 Score Thresholding

The recognisability threshold is enforced at the extraction stage by only selecting the regional maxima whose NavGrid score meets or exceeds the minimum recognisability threshold:

$$\text{NavScore}(c) \geq \tau_{\text{rec}} = 0.5 \tag{18}$$

This ensures that only cells meeting or exceeding the navigability score are qualified for being intermediate waypoint or observation point candidates. The threshold $\tau_{\text{rec}} = 0.5$ was selected empirically by taking the lower values as the candidates which can not be confidently recognised and higher value as the candidates which can be highly recognised.

4.3.3 Non-Maximum Suppression

To prevent candidates from being densely populated within the same terrain patch, which would contribute almost nothing to the success of the operation, a minimum spacing constraint is applied. Five cells of intervals have initially applied, which can be changed according to user preferences. This minimum spacing implies the physical extent of $5 \times 175 = 875\,\text{px}$ in full-map coordinates. Following these three steps, **159 candidate nodes** were extracted from the NavGrid. Each node is stored as a row in the `WaypointNodes` table as listed in Table 1.

Table 1 Attributes stored for each of the 159 candidate waypoint nodes in `WaypointNodes`.

Attribute	Type	Description
`FullMapX`	Float	x-coordinate of the cell centre in full-map pixel coordinates.
`FullMapY`	Float	y-coordinate of the cell centre in full-map pixel coordinates.
`NavScore`	Float	Normalised navigability score of the cell, NavGrid $\in [0, 1]$.
`GridRow`	Integer	Row index of the cell in the 190×190 navigability grid.
`GridCol`	Integer	Column index of the cell in the 190×190 navigability grid.

4.3.4 Inter-Node Cost Matrix

To support route cost evaluation by the solver algorithm in stage 3, a 159×159 cost matrix is precomputed between all pairs of candidate nodes. The cost between nodes i and j is calculated as the product of the Euclidean pixel distance between them and the mean CostGrid value of the straight-line path connecting them:

$$\text{CostMatrix}(i, j) = \text{dist}(i, j) \times \frac{1}{P} \sum_{p=1}^{P} \text{CostGrid}(c(\mathbf{r}_{ij}(p))) \tag{19}$$

where $\text{dist}(i, j)$ is the pixel's Euclidean distance between nodes i and j, $P = 50$ is the number of equidistant sample points along the straight line path between them, $\mathbf{r}_{ij}(p)$

is the p-th sample point coordinate, and $c(\cdot)$ maps a coordinate to its respective grid cell.

4.4 Optimisation

The two outer optimisation approaches used the same A* route evaluator. NSGA-II [21] optimises f_1 and f_2 as separate objectives with its multi-objective solver capability and non-dominated waypoint assignments. The GA-mTSP method instead used the scalarised objective for the multi-objective framework such that:

$$F = \omega_1 f_1 + \omega_2 f_2, \tag{20}$$

with seven weight combinations ranging from pure reliability (f_1) to pure coverage (f_2).

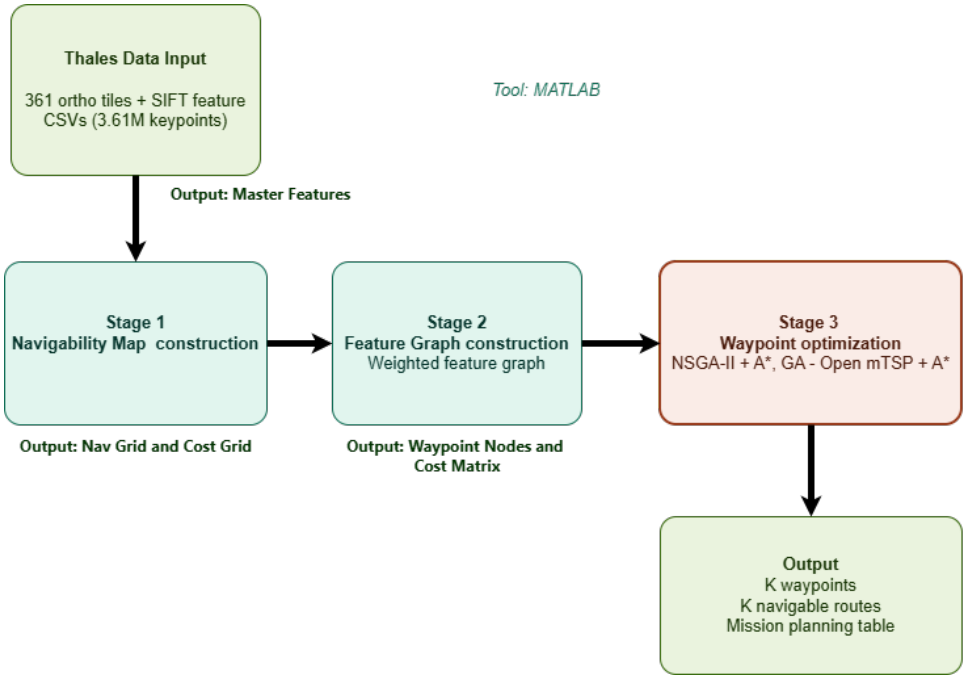


Fig. 1 Methodology from orthomosaic imagery and SIFT features to terrain navigability mapping, route planning, and multi-UAV waypoint assignment.

5 Results and Discussion

5.1 Baseline Results

NSGA-II + A^* was evaluated at $K = 5$ and returned 50 non-dominated solutions. Under the baseline configuration, all solutions converged to

$$f_1 = 0.3770, \qquad f_2 = 0.9098. \tag{21}$$

While GA-mTSP + A^* achieved

$$f_1 = 0.3707, \qquad f_2 = 0.9098. \tag{22}$$

Table 2 summarises the comparison. The two solvers (NSGA-II + A^*, GA-mTSP + A^*

Table 2 Baseline solver comparison at $K = 5$.

Solver	f_1	f_2 (%)	Time (s)
NSGA-II + A^*	0.3770	90.98	113.9
GA-mTSP + A^*	0.3707	90.98	725.6

) produced nearly identical results of $f_1 = 0.3770$,$f_1 = 0.3770$ respectively, and both at the same $f_2 = 91.0\%$ coverage. Both solvers identified UAV 5, assigned to terminal w_{130}, as the weakest route. Its mean calibration gap was exceeding the threshold set, which reduced its penalty factor to

$$\lambda_5 = 0.947. \tag{23}$$

NSGA-II produced these results in a single run with the Pareto-native approach at one-fifth of GA-mTSP's total computational cost across the tests conducted. Both solvers independently identified $K_{\text{BEST}} = 5$ the swarm size, which is achieving the possible maximum coverage under this configuration.

5.2 Altitude-Adjusted Coverage

At the base altitude of 100 m, the five UAVs' cameras cover 37.6% the border in union, with 6 gaps identified as NSGA-II results before altitude adjustment, and after altitude adjustment, the final union reaches 91.0% of the border, a coverage gain of 53.4%. Table 3 shows the adjusted altitudes for each UAV, and Figure 2 shows the routes and coverage on the operational ortho-imagery. UAVs 4 and 5 reached the maximum H_MAX = 300 m, UAV 3 requires the least altitude increase up to 231 m of the five in this run, and all others have been adjusted from base altitude for covering the identified gap.

Table 3 Per-UAV altitude assignments for the nearest-to-ideal solution (K=5).

UAV	Terminal	Altitude (m)
1	w48	266
2	w73	266
3	w55	231
4	w9	300
5	w130	300

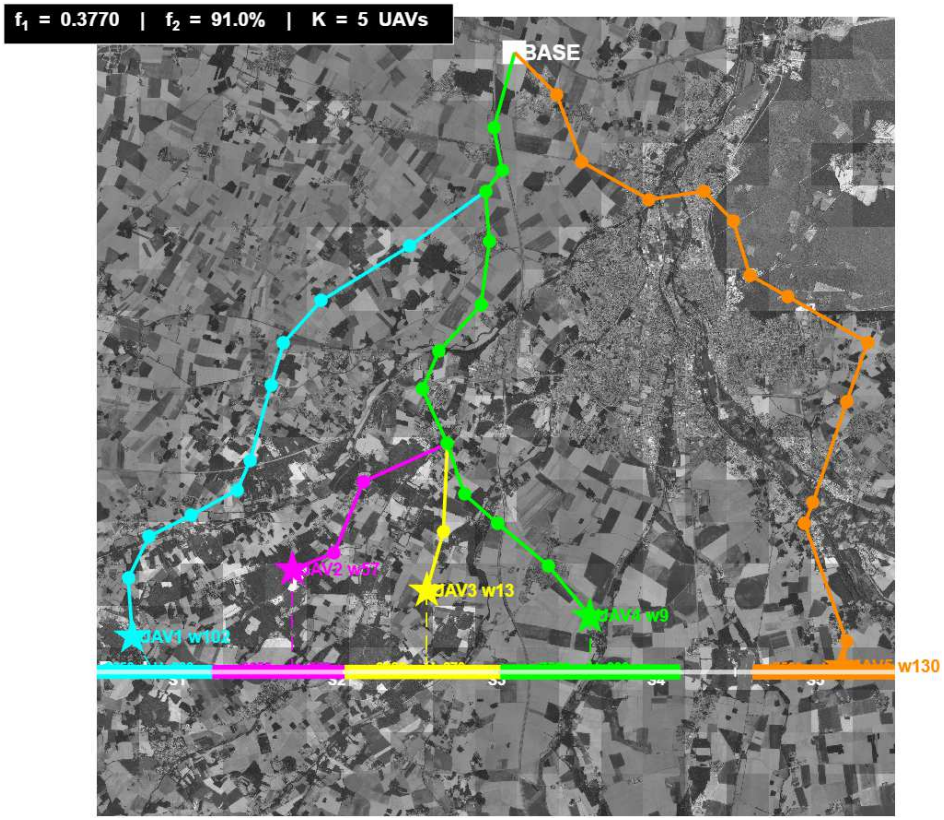


Fig. 2 NSGA-II + A^* mission map for $K = 5$, showing routes, terminal observation points, and altitude-adjusted surveillance footprints.

5.3 Swarm-Size Analysis

The swarm size was varied from $K = 1$ to $K = 8$. Table 4 reports each swarm size coverage $f_2(K)$ for both solvers. Figures 3 and 4 show the resulting coverage curves. The coverage curves are the same for both solvers at every swarm size tested, despite

Table 4 Swarm-size sweep results for both solvers.

	NSGA-II + A*		GA-mTSP + A*		
K	f_2 (%)	Δf_2	f_2 (%)	Δf_2	Marker
1	22.6	–	22.6	–	
2	45.1	+22.6	45.1	+22.6	
3	63.0	+17.9	63.0	+17.9	
4	85.5	+22.6	85.5	+22.6	
5	91.0	+5.5	91.0	+5.5	K_{BEST} (both solvers)
6	91.0	+0.0	91.0	+0.0	
7	91.0	+0.0	91.0	+0.0	
8	91.0	+0.0	91.0	+0.0	

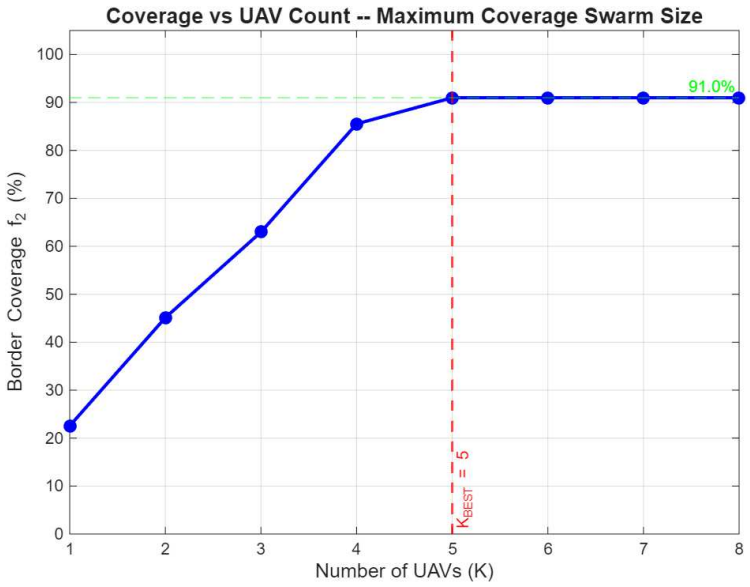


Fig. 3 NSGA-II + A^* coverage vs. swarm size.

using different search mechanisms. From $K = 1$ to $K = 4$ there is a sharp increase in coverage, where each additional UAV adds between 5.5 and 22.6 percentage points before stops increase exactly at $K = 5$ which the marginal gain from $K = 4$ to $K = 5$ drops to 5.5% and remains at 0.0% for every consecutive additional swarm size tested. Both solvers' swarm size optimisation terminated for the same reason: three consecutive swarm-size increases ($K = 6, 7, 8$) each returns a marginal gain below the 2% which was taken as the returns threshold for three consecutive swarm size returns.

$$K_{\text{BEST}} = \arg\max_{K} f_2(K) = 5, \qquad f_2(K_{\text{BEST}}) = 91.0\% \tag{24}$$

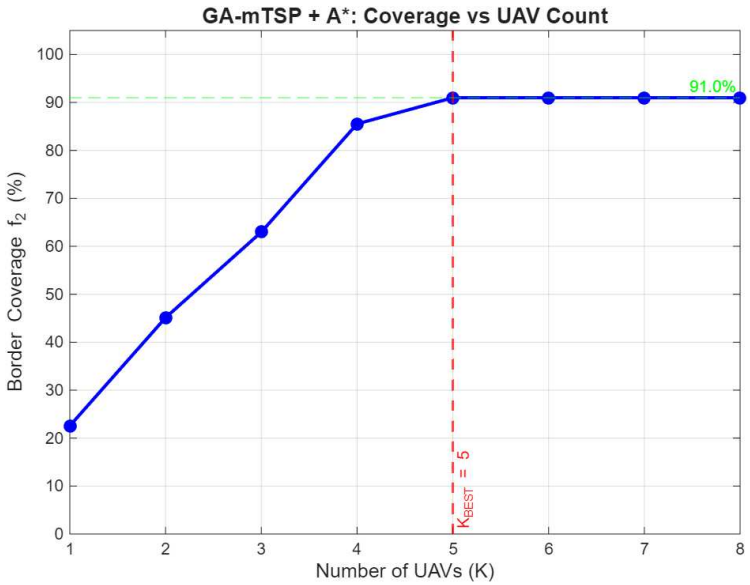


Fig. 4 GA-mTSP + A^* coverage vs. swarm size.

This is the same for both solvers, although the total time to reach this conclusion is different: NSGA-II + A^* completed its eight swarm sizes in 1007.4 s, while GA-mTSP + A^* spend 5559.0 s on the same 5.5× gap in computation discussed above.

5.4 Parameter Sensitivity

The increase in routing-graph connectivity from $K_{\mathrm{NN}} = 4$ to $K_{\mathrm{NN}} = 15$ resulted in a reduction of NSGA-II reliability from 0.3770 to 0.2226 and from 0.3707 to 0.2175 for GA-mTSP reliability. This is due to the fact that the increased connectivity allowed A* to generate shorter routes with fewer intermediate nodes and resulted in a large penalty from increased spacing between connected nodes. This shows that a shorter distance route was not necessarily a reliable route for visual navigation. The influence of α was also investigated. The changing of alpha shows that the coverage remained

Table 5 Sensitivity of route reliability to α.

α	NSGA-II f_1	GA-mTSP f_1
0.0	0.1460	0.1333
0.3	0.2846	0.2757
0.5	0.3770	0.3707
0.8	0.5157	0.5132
1.0	0.6081	0.6081

unchanged at 91.0% because α affects route navigability rather than the observation

footprint. Further parameter sensitivity in Altitude shows that reducing the maximum observation altitude from 300 m to 120 m increased the coverage and increased the swarm size from five to sixteen UAVs.

5.5 Discussion

The results demonstrate that terrain visual navigability affects multi-UAV mission planning in ways not represented by geometric path length alone. Increasing graph connectivity produced shorter routes but with a cost of approximately 41% reduction in the route-reliability objective because the spacing between recognisable calibration locations increased. The results of NSGA-II and GA-mTSP independently agree that under the same baseline parameters they produced the same weakest route and swarm-size coverage. This indicates that the main influence of the result is terrain-dependent formulation rather than the choice of outer optimisation algorithm.

The main difference was computational cost due to the fact that NSGA-II searched both objectives simultaneously while GA-mTSP repeated the optimisation across seven scalarisation weights and took large total computation time in comparison with NSGA-II. The 91.0% coverage ceiling is valid, as only 159 candidate navigation nodes were selected from 3.6 million SIFT keypoints following the recognisability threshold. Some border regions contained no suitable observation position, so adding more UAVs contributes nothing to resolve the identified gaps.

6 Conclusion and Future Work

This work addressed the waypoint-assignment problem for UAV swarms conducting border surveillance in GNSS-denied environments. A terrain navigability scoring framework was developed from orthomosaic imagery by combining SIFT feature density and response quality, and the resulting navigability map was used during route planning and observation-point selection.

The waypoint-assignment problem was formulated using weakest-link route reliability and collective border coverage objectives and evaluated using two independent optimisation approaches sharing the same A^* routing mechanism. Under the baseline configuration, NSGA-II + A^* achieved

$$(f_1, f_2) = (0.3770, 0.9098), \tag{25}$$

while GA-mTSP + A^* achieved

$$(f_1, f_2) = (0.3707, 0.9098). \tag{26}$$

Both methods identified $K_{\mathrm{BEST}} = 5$ approximately 91.0% maximum baseline coverage. Their agreement indicates that the principal behaviour of the solutions is associated with the physical terrain navigability and coverage characteristics represented in the formulation. The sensitivity analysis showed that shorter geometric routes are not always preferable for visual navigation. Increasing routing connectivity reduced route

distance but increased the spacing between recognisable calibration points and reduced the weakest-link reliability score.

Future work should incorporate aircraft endurance directly into the optimisation and use real world recorded calibration distance, sensor, and altitude parameters. UAV real-world flight testing trials are required to validate whether the proposed terrain navigability score corresponds to actual localisation performance. Further development should also consider seasonal changes in terrain appearance, alternative image-processing or learned visual features, and online replanning when the environment observed during flight differs from the pre-mission map.

Acknowledgements. The author acknowledges the Institut national de l'information géographique et forestière (IGN), France, as the source of the orthophoto imagery used in this study. The author also acknowledges Thales UK for collaboration on the Individual Research Project and for facilitating access to the project data inputs, including the associated pre-extracted SIFT feature data. The author further acknowledges Mr Darren Price for his support as the Thales representative throughout the project.

Declarations

Funding

This research received no specific funding.

Conflict of interest/Competing interests

The authors declare that they have no relevant financial or non-financial interests to disclose.

Ethics approval and consent to participate

Ethical approval for this study was obtained from Cranfield University. As the study did not involve human participants, consent to participate was not applicable.

Consent for publication

Not applicable.

Data availability

The operational orthomosaic imagery and SIFT feature dataset used in this study were provided by Thales UK. These data are not publicly available due to applicable access and data-sharing restrictions.

Materials availability

No physical research materials were generated or used in this study beyond the datasets and computational resources described above. Therefore, materials availability is not applicable.

Code availability

The MATLAB code developed for this study is maintained in a private GitHub repository. Access to the code may be provided by the corresponding author upon reasonable request, subject to any applicable project and data-sharing restrictions.

Author Contributions

Jean Marie Vianney ISHIMWE: Methodology, software, simulation, data analysis, investigation, visualisation, and writing—original draft.

Sabyasachi Mondal: Supervision, conceptual guidance, technical advice, validation, and writing—review and editing.

Antonios Tsourdos: Supervision, manuscript review, critical feedback, and writing—review.

References

[1] Ahmadian, N., Lim, G.J., Torabbeigi, M., Kim, S.J.: Smart border patrol using drones and wireless charging system under budget limitation. Computers & Industrial Engineering **164**, 107891 (2022) https://doi.org/10.1016/j.cie.2021.107891

[2] Nordic, E., *et al.*: Jamming and spoofing techniques for drone neutralization: An experimental study. Drones **8**(12), 743 (2024) https://doi.org/10.3390/drones8120743

[3] Burbank, J., Greene, T., Kaabouch, N.: Detecting and mitigating attacks on GPS devices. Sensors **24**(17), 5529 (2024) https://doi.org/10.3390/s24175529 . PMCID: PMC11397858

[4] Lu, Y., Xue, Z., Xia, G.-S., Zhang, L.: A survey on vision-based uav navigation. Geo-spatial Information Science **21**(1), 21–32 (2018) https://doi.org/10.1080/10095020.2017.1420509 https://doi.org/10.1080/10095020.2017.1420509

[5] Arafat, M.Y., Alam, M.M., Moh, S.: Vision-based navigation techniques for unmanned aerial vehicles: Review and challenges. Drones **7**(2) (2023) https://doi.org/10.3390/drones7020089

[6] Liu, K., Zhou, H., Xu, R., Wang, P., Song, M., Zhang, H.: Beyond matching to tiles: Bridging unaligned aerial and satellite views for vision-only uav navigation. In: Proceedings of the IEEE/CVF Conference on Computer Vision and Pattern Recognition (CVPR), pp. 5359–5368 (2026)

[7] Thoma, J., Paudel, D.P., Chhatkuli, A., Probst, T., Van Gool, L.: Mapping, localization and path planning for image-based navigation using visual features and map. In: Proceedings of the IEEE/CVF Conference on Computer Vision and Pattern Recognition (CVPR) (2019). https://doi.org/10.1109/CVPR.2019.00756

[8] Mur-Artal, R., Tardós, J.D.: ORB-SLAM2: An open-source SLAM system for monocular, stereo, and RGB-D cameras. IEEE Transactions on Robotics **33**(5), 1255–1262 (2017) https://doi.org/10.1109/TRO.2017.2705103

[9] Qin, T., Li, P., Shen, S.: Vins-mono: A robust and versatile monocular visual-inertial state estimator. IEEE Transactions on Robotics **34**(4), 1004–1020 (2018) https://doi.org/10.1109/TRO.2018.2853729

[10] Gallo, E., Barrientos, A.: GNSS-Denied Semi Direct Visual Navigation for Autonomous UAVs Aided by PI-Inspired Inertial Priors. arXiv preprint arXiv:2205.13242 (2022). https://arxiv.org/abs/2205.13242

[11] Lajoie, P.-Y., Hu, S., Beltrame, G., Carlone, L.: Modeling perceptual aliasing in SLAM via discrete-continuous graphical models. IEEE Robotics and Automation Letters **4**(2), 1435–1442 (2019) https://doi.org/10.1109/LRA.2019.2895450

[12] Brossard, M., *et al.*: Deployment of reliable visual inertial odometry approaches for unmanned aerial vehicles in real-world environments. In: Proceedings of the International Conference on Unmanned Aircraft Systems (ICUAS) (2022). arXiv:2302.01867

[13] Hart, P.E., Nilsson, N.J., Raphael, B.: A formal basis for the heuristic determination of minimum cost paths. IEEE Transactions on Systems Science and Cybernetics **4**(2), 100–107 (1968) https://doi.org/10.1109/TSSC.1968.300136

[14] Sundar, K., Srinivasan, S., Misra, S., Rathinam, S., Sharma, R.: Landmark Placement for Localization in a GPS-Denied Environment. arXiv preprint arXiv:1802.07652 (2018). https://arxiv.org/pdf/1802.07652

[15] Costante, G., Forster, C., Delmerico, J., Valigi, P., Scaramuzza, D.: Perception-aware path planning. arXiv preprint arXiv:1605.04151 (2016) https://doi.org/10.48550/arXiv.1605.04151

[16] Wang, Z., *et al.*: Landmark selection and path planning for unmanned vehicles with position error corrections. Transportation Research Part C: Emerging Technologies (2023) https://doi.org/10.1016/j.trc.2023.104218

[17] Khattab, M., *et al.*: A global coverage path planning method for multi-UAV maritime surveillance in complex obstacle environments. Drones **8**(12), 764 (2024) https://doi.org/10.3390/drones8120764

[18] Holt, R.S., Beard, R.W.: Vision-based road-following using proportional navigation. Journal of Intelligent and Robotic Systems **57**(1–4), 193–216 (2010) https://doi.org/10.1007/s10846-009-9353-7

[19] Trigui, S., Cheikhrouhou, O., Koubaa, A., Baroudi, U., Youssef, H.: FL-MTSP: A fuzzy logic approach to solve the multi-objective multiple traveling salesman

problem for multi-robot systems. Soft Computing **21**(24), 7351–7362 (2017) https://doi.org/10.1007/s00500-016-2279-7

[20] Bektas, T.: The multiple traveling salesman problem: An overview of formulations and solution procedures. Omega **34**(3), 209–219 (2006) https://doi.org/10.1016/j.omega.2004.10.004

[21] Deb, K., Pratap, A., Agarwal, S., Meyarivan, T.: A fast and elitist multiobjective genetic algorithm: NSGA-II. IEEE Transactions on Evolutionary Computation **6**(2), 182–197 (2002) https://doi.org/10.1109/4235.996017

[22] Ghambari, S., Golabi, M., Lepagnot, J., Brévilliers, M., Jourdan, L., Idoumghar, L.: An enhanced NSGA-II for multiobjective UAV path planning in urban environments. In: Proceedings of the IEEE 32nd International Conference on Tools with Artificial Intelligence (ICTAI), pp. 106–111 (2020). https://doi.org/10.1109/ICTAI50040.2020.00027

[23] Huang, X.: NSGA-II algorithm in path planning of multiple unmanned aerial vehicle collaborative search tasks. In: Proceedings of the 2024 International Conference on Machine Intelligence and Digital Applications (MIDA) (2024). https://doi.org/10.1145/3662739.3670222